https://doi.org/10.5194/egusphere-2026-6383
Preprint. Discussion started: 9 November 2026
© Author(s) 2026. CC BY 4.0 License.

Representation of North Atlantic Atmospheric Rivers in the IFS and ICON Models: Insights from NAWDIC Dropsonde Observations

Magdalena Kracheletz[1], Joaquim G. Pinto[1], David A. Lavers[2], and Alexandre M. Ramos[1]

[1]Institute of Meteorology and Climate Research Troposphere Research (IMKTRO), Karlsruhe Institute of Technology (KIT), Karlsruhe, Germany
[2]European Centre for Medium-Range Weather Forecasts (ECMWF), Reading, UK

Correspondence: Magdalena Kracheletz (magdalena.kracheletz@kit.edu)

Abstract. Atmospheric Rivers (ARs), defined as narrow bands of intense water vapor transport, are a major driver of wintertime heavy precipitation and flood events across Western Europe. Due to the high impacts of ARs, accurate forecasts are crucial, but their initialization and evaluation remains challenging due to a lack of observational data over the oceans. The “North Atlantic Waveguide, Dry Intrusion and Downstream Impact Campaign" (NAWDIC) collected unique dropsonde observations of several strong ARs that caused widespread flooding, disruption and economic damage over the Iberian Peninsula and Northern Africa in January and February 2026 .

Using this one-of-a-kind dataset, we performed the first systematic evaluation of the AR representation over the North Atlantic ocean basin in the IFS and the ICON models. Specifically, the vertical structure of temperature, specific humidity, horizontal wind speed, and moisture flux magnitude was analyzed using the model data assimilation outputs. While the overall representation of ARs in the IFS and ICON models is skillfull, results indicate large random errors in the horizontal wind speed estimates and a slight cold bias over North Atlantic AR regions. The IFS exhibits an underestimation and large random errors in the humidity, peaking between 700 and 750 hPa, which corresponds to the upper-level extension of ARs. The ICON model tends to slightly underestimate the humidity throughout the boundary layer and the entire lower troposphere up to 650 hPa. The large random errors in wind speed and the underestimation of humidity in both models lead to an underestimated and highly uncertain moisture flux magnitude in the IFS and ICON models. The results of this study highlight the importance of observational data from AR regions over the North Atlantic and the current model limitations in accurately representing intense ARs affecting Western Europe.

1 Introduction

Flood events resulting from heavy precipitation are a major hazard affecting Western and Central Europe (e.g. Barredo, 2007; Marchi et al., 2010; Hofstätter et al., 2018) that frequently causes substantial damage, disruption, economic losses and fatalities (e.g. Paprotny et al., 2018; Ludwig et al., 2023). In the extended winter period, flood events can be connected to the occurrence of Atmospheric Rivers (ARs) (e.g. Waliser and Guan, 2017; Eiras-Barca et al., 2018; Ionita et al., 2020; Ferreira et al., 2025, 2026). ARs are defined as elongated, narrow corridors of strong horizontal water vapor transport, and account for the largest transport of freshwater on Earth (Ralph et al., 2018).

https://doi.org/10.5194/egusphere-2026-6383
Preprint. Discussion started: 9 November 2026
© Author(s) 2026. CC BY 4.0 License.

In the mid-latitude regions, ARs are highly linked to extratropical cyclones (ETCs) (Dacre et al., 2015; Ralph et al., 2018; Zhang et al., 2019). The ETCs affecting Western Europe often originate from disturbances at the polar front over the North Atlantic ocean (Bjerknes, 1919) and intensify while traveling eastwards towards the Western European coast (e.g. Fink et al., 2009). ETCs typically develop a frontal system containing the warm front, followed by the cold front, which define the boarders of the warm sector (Schultz et al., 2019). The developing characteristic air streams around an ETC can be described using the model of conveyor belts (Carlson, 1980; Schultz, 2001). The cold conveyor belt originates from the lower troposphere, passes on the poleward side underneath the warm frontal zone, wraps around the core and can cause strong winds at the surface (Schultz, 2001; Martínez-Alvarado et al., 2014). The dry intrusion air stream (DI) descends from the upper troposphere towards the surface near boundary layer (Young et al., 1987). It can cause damaging high wind gusts at the surface and can further enhance the moisture uptake over the ocean in the region of the DI outflow (e.g. Quinting et al., 2026). The warm conveyor belt (WCB) travels parallel to and ahead of the ETC cold front towards the cyclone center in the warm sector, before it ascends over the warm front. The condensation of its often moist air masses produces precipitation as well as diabatic heating that further intensifies the cyclone (Browning, 1971). Often located in the same area as the WCB lies the AR. It forms its elongated structure ahead of the ETC's cold front, and gathers moisture often from tropical and subtropical sources (Ramos et al., 2016), as well as the moisture the cold front sweeps up on its way over the extra-tropical ocean (Dacre et al., 2015; Dacre and Clark, 2025). When the highly moist AR air masses are lifted in the ascending WCB, or by orographic lifting, ARs can cause heavy precipitation (Dacre et al., 2015; Ralph et al., 2018). If this lifting takes place after the AR made landfall over the continent, the impacts for the affected regions are high (e.g. Eiras-Barca et al., 2018). Therefore accurate predictions of the AR landfall position and the expected amount of precipitation are crucial for weather warnings, impact forecasting and risk management (e.g. Ramos et al., 2020; Merz et al., 2020).

The numerical weather prediction (NWP) forecasts of ETCs and their associated ARs improved a lot over the past years (e.g. DeFlorio et al., 2018; ECMWF, 2026). However, AR forecasts can still exhibit systematic and random errors, whose magnitude depends on the region and on the considered variable (Yu et al., 2025). Several studies identified an underestimation of moisture transport in the short-term forecast (12 h) during AR events, caused by a dry bias and a low-level weaker wind bias in models during the winter season over the mid-latitude oceans (Lavers et al., 2020a; Yu et al., 2025). This is accompanied by a cold bias in AR air masses traveling over the Northern Hemisphere oceans in the winter period (Lavers et al., 2020a; Yu et al., 2025). Additionally, model random errors of especially moisture are higher for AR forecasts than for the forecast climatology (Lavers et al., 2018; Yu et al., 2025). The exact AR landfall position is often wrongly predicted for forecast lead times above 5 days, especially over the Iberian Peninsula (Ramos et al., 2020), and a dry bias is found for several regions along the European west coast during AR passages (Ramos et al., 2026).

The scarcity of observational data over the oceans, where ARs evolve and intensify, poses a significant challenge for operational forecasts, as well as for the evaluation of the forecasts and the identification of biases in the forecast models. Due to the lack of measurements, the NWP models can sometimes be poorly constrained by observations in the data assimilation procedure and their forecasts cannot be verified afterwards by comparing them against observational data. A key factor in the evaluation and improvement of AR forecasts are therefore observational campaigns that directly target ARs over the oceans. In

https://doi.org/10.5194/egusphere-2026-6383
Preprint. Discussion started: 9 November 2026
© Author(s) 2026. CC BY 4.0 License.

the past years, several campaigns sampled directly or indirectly ARs in the different oceanic basins around the globe, such as in the Arctic regions (Wendisch et al., 2019; Mech et al., 2022; Wendisch et al., 2024), on the Southern Hemisphere in the Indian Ocean (https://www.eol.ucar.edu/field_projects/socrates, https://halo-research.de/science/halo-missions/halo-south/) and in the mid-latitudes of the Northern Hemisphere in the Pacific and the North Atlantic ocean (Wick et al., 2018; Schäfler et al., 2018; Ralph et al., 2020; Zheng et al., 2025). A continuous achievement is made by the Atmospheric River Reconnaissance Campaign (AR Recon), which is an observational campaign designed to improve flood forecasting over the US by enhanced dropsonde observations of ARs in the Eastern Pacific and Western Atlantic (Ralph et al., 2020; Zheng et al., 2025). It first took place in 2016, and has become operationally in 2020, nowadays making use of several research aircraft and other measuring platforms like a net of drifting buoys each winter (Ralph et al., 2020). AR Recon data significantly improved precipitation forecasts over the AR landfall regions in the US (Zheng et al., 2021; Wang et al., 2026) and helped to identify model biases over AR regions (e.g. Lavers et al., 2018, 2020a). The North Atlantic Waveguide and Downstream Impact Experiment (NAWDEX), which took place in autumn 2016, studied diabatic processes in North Atlantic ETCs and the influence on downstream High Impact Weather with several research aircraft (Schäfler et al., 2018). It contributed largely to the understanding of ETC dynamics in the North Atlantic basin and their downstream impacts over Europe (e.g. Schäfler et al., 2020; Harvey et al., 2020).

As ARs were not a direct aim of the 10-year old NAWDEX campaign, and other campaigns in the North Atlantic, such as the HALO-$(AC)^3$ campaign in 2022 (Wendisch et al., 2024), focused more on ARs affecting the Arctic regions, the need for an interdisciplinary European-American field campaign targeting North Atlantic ARs that affect the Western European coast became apparent (Lavers et al., 2020b). Such a campaign was carried out in the winter of 2025/2026 within the "North Atlantic Wave Guide, Dry Intrusion, and Downstream Impact Campaign" (NAWDIC) (https://www.nawdic.kit.edu/). The NAWDIC campaign was an international, joint effort to improve the process understanding and modeling of ETC dynamics by collecting detailed observations over the North Atlantic and Western Europe using several research aircraft and ground based measurements (Quinting et al., 2026). In addition to the main focus on the sampling of the mesoscale tropopause structure, the interaction of the DI with the planetary boundary layer (PBL), and the influence on High Impact Weather over the European continent, NAWDIC aimed to improve AR forecasts with enhanced observations in regions of moisture uptake and moisture transport.

For several weeks during the NAWDIC campaign time frame from 13 January to 20 February 2026, the large-scale weather situation over the North Atlantic was dominated by Greenland blocking (Grams, 2026), which guided the ETCs and their corresponding ARs on a southerly path towards the Iberian Peninsular and Northern Africa. Several landfalling ARs, which contributed to the intensive floodings over Spain, Portugal and Morocco in February 2026 (e.g. Instituto Português do Mar e da Atmosfera, 2026a; Agencia Estatal de Meteorología, 2026), were sampled by NAWDIC with dropsondes released from the High Altitude and Long Range research aircraft (HALO) during six Intensive Observation Periods (IOPs). The collected dropsonde observations were assimilated in real time in the operational forecasts of the ECMWF's Intergrated Forecasting System (IFS) (ECMWF, 2025) and the Icosahedral Nonhydrostatic Model (ICON) (Zängl et al., 2015), run by the German Weather Agency (DWD).

https://doi.org/10.5194/egusphere-2026-6383
Preprint. Discussion started: 9 November 2026
© Author(s) 2026. CC BY 4.0 License.

We make use of this unique dropsonde data to investigate the representation of impactful North Atlantic ARs in the IFS and the ICON models. Previous assessments of AR representation in the IFS have focused either on the eastern North Pacific (Lavers et al., 2018, 2020a), or on landfalling ARs, such as over Europe (Ramos et al., 2026), but an assessment for ARs in the IFS over the North Atlantic has not yet been undertaken. Evaluations of AR representation in the ICON model have so far only been limited to high-resolution case studies of ARs in the Arctic region (Bresson et al., 2022). To date, no systematical assessment of AR representation in the operational global ICON model has been conducted. This study therefore provides the first evaluation of IFS and ICON model performance with respect to their ability to represent the vertical structure of North Atlantic ARs affecting the Western European coast. Specifically, we compare the NAWDIC dropsonde observations to the IFS and ICON model estimates before and after the data assimilation (first guess and analysis) to answer two research questions:

1. How well do the IFS and ICON models represent the vertical structure of selected, impactful AR events over the North Atlantic during the NAWDIC campaign?

2. To what extent does data assimilation improve the model analysis relative to the first guess estimates over North Atlantic AR regions?

Sect. 2 provides an overview of the used datasets and methods in this study, including the methods used to characterize the synoptic situation regarding ARs during the NAWDIC campaign (Sect. 2.1), the presentation of the available NAWDIC AR dropsonde data (Sect. 2.2), and an introduction on the structure of the IFS and ICON data assimilation feedback files (Sect. 2.3), as well as the in this study performed calculations on the feedback data (Sect. 2.4). The large-scale weather situation during late January and beginning of February 2026 is described in Sect. 3. The main results are presented in Sect. 4, including two case studies of selected NAWDIC IOPs (Sect. 4.1 and Sect. 4.2), and a general assessment of the IFS and ICON model performance over AR regions (Sect. 4.3). A discussion of the results is provided in Sect. 5, followed by a summary and conclusion of this studies results in Sect. 6.

2 Data and Methods

2.1 ERA5 Reanalysis Data

The synoptic situation over the North Atlantic is assessed using the ERA5 reanalysis dataset (Hersbach et al., 2020), provided by the ECMWF. Used variables are the mean sea level pressure in hPa, the u wind component in the $250\,\mathrm{hPa}$ level in $\mathrm{m\,s^{-1}}$, and the eastward and northward component of the integrated water vapor flux in $\mathrm{kg\,m^{-1}\,s^{-1}}$, from which the integrated water vapor transport (IVT) is computed.

To compare the large-scale weather situation during the NAWDIC campaign to the climatology, we evaluate two subsets: The 30-day period from 19 January to 19 February 2026, where NAWDIC IOPs targeting ARs took place, and for comparison all winter months December, January, and February (DJF) from the years 1984 to 2024. To derive the climatology of the polar jet stream and the IVT distribution over the North Atlantic, we compute 40-year DJF composites over the $250\,\mathrm{hPa}$ u wind

https://doi.org/10.5194/egusphere-2026-6383
Preprint. Discussion started: 9 November 2026
© Author(s) 2026. CC BY 4.0 License.

component and the IVT field. The u wind component in 250 hPa is often used as a measure for the jet stream location and strength (e.g. Santos et al., 2013). The climatology composite of jet stream and IVT is then substracted from the composite over the 30-day campaign period to assess the anomalies of the jet stream and the AR activity during the NAWDIC campaign. The significance of the anomalies is tested by comparing the monthly average of the campaign time frame to the monthly averages over the 40-year winter months and classifying values as significant if they exceed the 95 percentile. To display the evolution of IVT over the North Atlantic during January and February, a Hovmoeller plot, averaging the IVT between 30 °N and 55 °N, is created (Sect. 3).

2.2 NAWDIC Campaign and AR Dropsonde Observations

As part of the NAWDIC campaign (https://www.nawdic.kit.edu/), the research aircraft HALO, operated by the German Aerospace Center (DLR), was based in Shannon, Ireland from 13 January to 20 February 2026. During the six-week campaign period, HALO conducted 18 research flights over the North Atlantic. The aircraft was equipped with a variety of measuring instruments, including the KITsonde dropsonde system (Kottmeier et al., 2025). The KITsondes are designed to sample the mesoscale structure of the atmosphere. The modular deployment system can release up to four dropsondes with different fall-speeds simultaneously from a single release container. After release, the dropsondes separate horizontally and sample the vertical distribution of temperature, relative humidity, pressure and wind at their different locations with an uncertainty of <0.25 K, <3 %RH, <1 hPa and $<0.1\,\mathrm{m\,s^{-1}}$ (Graw, 2025) respectively, and a temporal resolution of 1-1.12 s (Kottmeier et al., 2025). Considering the data of only one dropsonde per drop makes the KITsonde data equivalent to that obtained from conventional dropsonde systems.

Six of the 18 NAWDIC IOPs focused on the sampling of ARs with dropsondes. These are IOP 4 “Dublin” on 20 January 2026, IOP 7 “Limerick” on 28 January 2026, IOP 11 “Sligo” on 3 February 2026, IOP 16 “Kilbeggan” on 14 February 2026, IOP 17 “Mallow” on 16 February 2026 and IOP 18 “Killaloe” on 17 February 2026 (Fig. 1). The ERA5 IVT distribution of the sampled ARs is shown in Fig. 1, together with the corresponding HALO flight tracks and the release locations of the dropsonde containers. A close-up of these maps, focusing on the HALO flight track and the dropsonde locations, can be found in Fig. 3, Fig. 4 and in the supplementary material in Fig. S1. From each successful release container during NAWDIC, the profile with the best data quality was selected from the two to four available dropsonde profiles and was transmitted to the WMO Information System 2.0 (WIS 2.0), which distributes meteorological observations for the data assimilation into NWP models.

To distinguish the dropsondes released over AR regions from the ones released into other ETC features, two criteria are applied: First, the ERA5 IVT at the dropsonde release location must exceed $200\,\mathrm{g\,kg^{-1}\ m\,s^{-1}}$ at the time of the drop. This threshold is lower than the usual threshold of $250\,\mathrm{g\,kg^{-1}\ m\,s^{-1}}$ (e.g. Ralph et al., 2018), to include a slightly larger set of dropsondes into the statistical calculations carried out later in this paper. Second, a quality control is performed to exclude the profiles that clearly exhibit cold front or cold sector features of the sampled ETC, even though the IVT is still above $200\,\mathrm{g\,kg^{-1}\ m\,s^{-1}}$. Following these two criteria, 44 of the in total 127 dropsonde containers released during NAWDIC, are

https://doi.org/10.5194/egusphere-2026-6383
Preprint. Discussion started: 9 November 2026
© Author(s) 2026. CC BY 4.0 License.

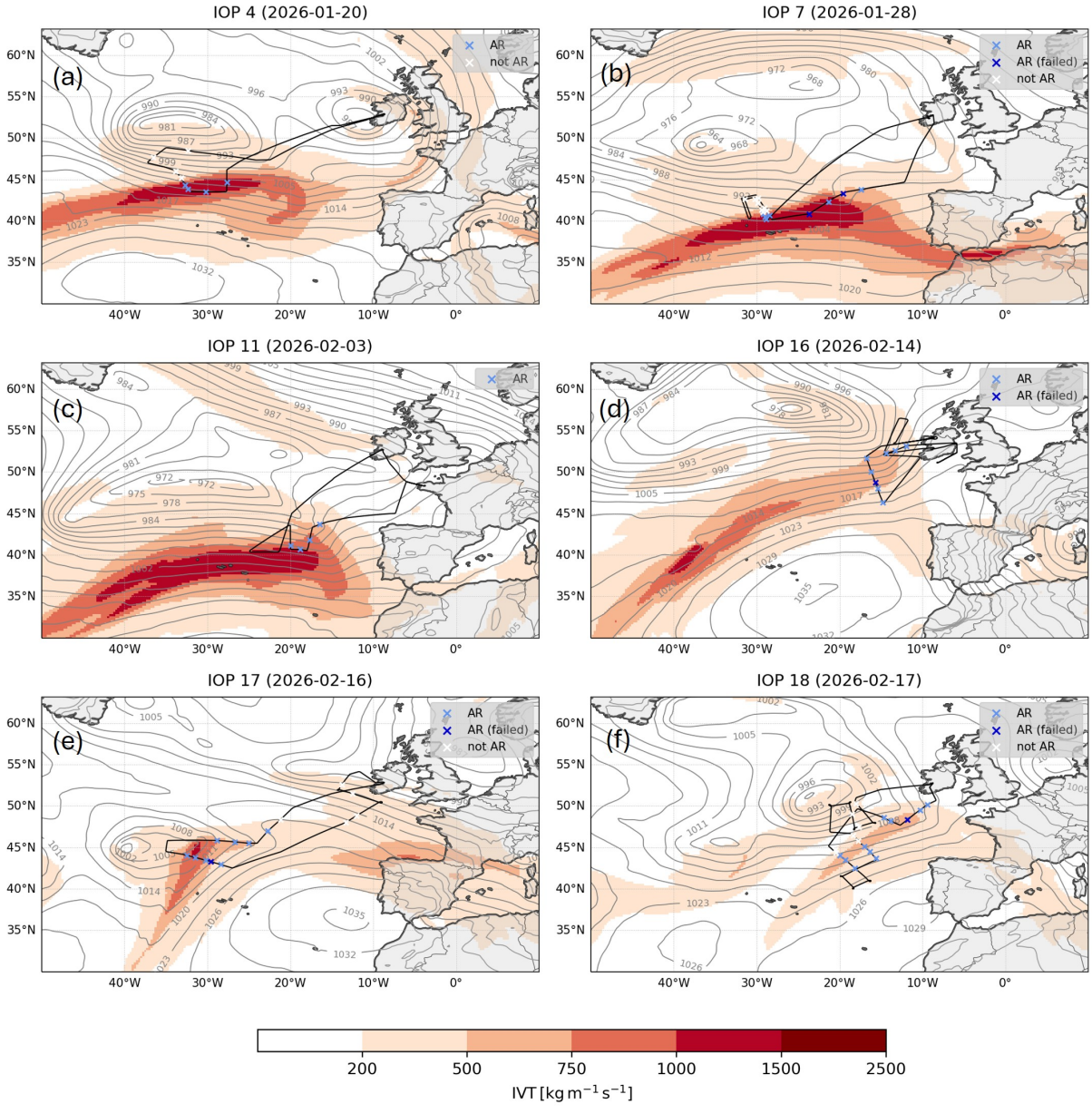


Figure 1. The HALO flight tracks of the six NAWDIC IOPs that sampled ARs are displayed on maps of ERA5 IVT (red shading) and mean sea level pressure (MLP) (contour lines). Panel (a): IOP 4 "Dublin" on 20 January 2026 (IVT and MLP valid at 12 UTC). Panel (b): IOP 7 "Limerick" on 28 January 2026 (valid at 14 UTC). Panel (c): IOP 11 "Sligo" on 3 February 2026 (valid at 14 UTC). Panel (d): IOP 16 "Kilbeggan" on 14 February 2026 (valid at 12 UTC). Panel (e): IOP 17 "Mallow" on 16 February 2026 (valid at 11 UTC). Panel (f): IOP 18 "Killaloe" on 17 February 2026 (valid at 11 UTC). Released dropsonde containers are marked with crosses on the flight track. The drops are divided into non-AR drops (white), AR drops that were transmitted to WIS 2.0 (light blue), and AR drops that were not sent to WIS 2.0 (dark blue) due to technical failures.

https://doi.org/10.5194/egusphere-2026-6383
Preprint. Discussion started: 9 November 2026
© Author(s) 2026. CC BY 4.0 License.

classified as AR drops. From these 44, only 39 containers, marked in light blue in Fig. 1, provided valuable observations. The remaining five containers, marked in dark blue, either failed to open or did not transmit usable data.

2.3 IFS and ICON Data Assimilation Procedures

In this study, we evaluate the Integrated Forecasting System (IFS, Cycle 49r1) run by the ECMWF (ECMWF, 2025) and the global, operational version of the Icosahedral Nonhydrostatic Model (ICON) (DWD, 2025) run by the DWD. The two NWP models were chosen because both assimilated the NAWDIC dropsonde data in real time. Further, both models are operationally used and are important contributors to the daily European weather forecasts. In the model data assimilation, the previous model forecast, called the first guess (FG), is updated using available observations (O) of the atmospheric state to create the best possible estimate of the atmospheric conditions. The corrected version of the FG is then called the analysis (AN) and is used as the initial condition for the next forecast run (e.g. Rabier, 2005; Kalnay, 2003).

The IFS uses a four dimensional variational (4D-Var) assimilation procedure that pulls the model trajectory in a finite assimilation window as closely as possible towards the observations while remaining consistent with physical model dynamics and error statistics (Rabier et al., 2000). In this study, the output from the long-window data assimilation system, which performs two assimilation windows per day, one from 09 UTC to 21 UTC and one from 21 UTC to 9 UTC the next day, was retrieved from the ECMWF Meteorological Archival and Retrieval System (MARS). Within the 12-hour assimilation window, 30-minute assimilation cycles are performed that update the FG and AN after each 30-minute time slot (ECMWF, 2024). The NAWDIC KITsonde profiles, which were transmitted in very high vertical resolution to the WIS 2.0, were thinned to model levels by the IFS system for the active assimilation of specific humidity, temperature, and wind in the IFS. Since the KITsondes were dropped at an altitude of around 8 km during NAWDIC, data was assimilated at the 70 lowest IFS model levels of the in total 137 model levels. Only 35 of the 39 transmitted NAWDIC AR dropsondes were actively assimilated into the IFS, as four were rejected. An overview over the assimilated sondes over ARs per NAWDIC IOP is presented in Table 1.

The ICON model (Zängl et al., 2015) uses a 3-hourly cycled Ensemble Variational data assimilation system (En-Var), which is a hybrid method consisting of an ensemble Kalman filter and a three-dimensional variational analysis (3D-Var) (Reinert et al., 2026). The procedure is carried out 3-hourly at every assimilation time step, leading to eight generated AN per day. From the 39 transmitted NAWDIC AR KITsondes, 26 profiles were assimilated in ICON using the relative humidity, temperature and wind closest to the 90 ICON model levels (compare Table 1). The remaining 13 profiles were rejected. The dropsonde release height of approximately 8 km results in the data assimilation at the lowest 43 model levels in the ICON model.

2.4 Evaluation of Model Performance

To assess the deviations between observations and model estimates, observation minus background differences (Desroziers et al., 2005) are a common analysis tool in the data assimilation community, often called “departures”. The FG departure is defined as the observation minus the FG (O-FG) for a single measurement in observation space. The AN departure is respectively defined as the observation minus the AN (O-AN) (e.g. Desroziers et al., 2005).

https://doi.org/10.5194/egusphere-2026-6383
Preprint. Discussion started: 9 November 2026
© Author(s) 2026. CC BY 4.0 License.

IOP	Date	Drops over ARs	Profiles sent to WIS 2.0	Assimilated in IFS	Assimilated in ICON
4 “Dublin”	2026-01-20	4	4	3	2
7 “Limerick”	2026-01-28	8	6	4	3
11 “Sligo”	2026-02-03	4	4	4	4
16 “Kilbeggan”	2026-02-14	8	7	7	4
17 “Mallow”	2026-02-16	9	8	8	4
18 “Killaloe”	2026-02-17	11	10	9	9
In total	-	44	39	35	26

Table 1. Overview over the released dropsonde containers over AR regions during the six AR IOPs of the NAWDIC campaign. Additionally to the total number of AR drops per IOP, the fraction that was transmitted to WIS 2.0 is displayed, as well as the number of dropsondes that were actively assimilated in the IFS and the ICON models.

The IFS FG and AN departures for specific humidity, temperature, u wind component and v wind component are directly provided in the ECMWF Mars system in the so-called feedback files. The magnitude of the horizontal wind speed can then be calculated from the u and v wind components, and the moisture flux magnitude from the product of the horizontal wind speed in $\mathrm{m\,s^{-1}}$ and the specific humidity in $\mathrm{g\,kg^{-1}}$. The ICON departures are calculated as the difference of the observation and the provided FG and AN estimates. The relative humidity estimates from the ICON model are converted into specific humidity, to retrieve comparable results for the humidity in the IFS and the ICON model. The moisture flux in ICON is calculated using the retrieved specific humidity and the wind speed.

It is important to assess the systematic and random errors in the FG and the AN of the two models compared to the NAWDIC dropsonde observations over ARs. To this end, we collect the FG and AN departure data for temperature, specific humidity, wind speed, and moisture flux magnitude from all assimilated AR dropsonde measurements, 35 dropsondes in the IFS and 26 in ICON, in vertical bins of 50 hPa width. Then we compute the mean (systematic errors) and standard deviation (random errors) over all departure values in the bin separately for each model, and for each variable. For a more structured discussion of the results, we divide the vertical layers into three sub-parts of the troposphere: the planetary boundary layer (PBL), approximately ranging from 1000 hPa to 900 hPa, the lower free troposphere defined from 900 hPa to 700 hPa, and the upper free troposphere for all values above 700 hPa.

3 The Synoptic Situation Regarding ARs During NAWDIC

During the NAWDIC campaign in January and February 2026, the synoptic situation over the North Atlantic was dominated by Greenland blocking that remained persistent for several weeks (not shown). The jet stream, usually located around 45 °N - 50 °N over the North Atlantic, was shifted significantly further to the south in the period from 19 January to 19 February 2026, the time period when AR flights were performed by NAWDIC (Fig. 2). The large positive anomalies in the jet stream strength around 40 °N (compare Fig. 2 (a) and (b)) stretched from the western part of the Atlantic to the east over the Iberian

https://doi.org/10.5194/egusphere-2026-6383
Preprint. Discussion started: 9 November 2026
© Author(s) 2026. CC BY 4.0 License.

Peninsula and into the Western Mediterranean. The northern regions of the North Atlantic, such as the region south of Iceland, experienced a weaker jet than climatologically observed, which is also consistent with the occurrence of Greenland Blocking.

The significant positive IVT anomalies in the southern part of the North Atlantic and over Southern Europe (Fig. 2 (b)) indicate a high AR activity in these regions during the period between 19 January and 19 February 2026. The southerly jet position steered several ETCs and their corresponding ARs further south than under usual conditions and guided them towards the Iberian Peninsula and Northern Africa. This series of intense ARs can also be found in the Hovmoeller diagram in Fig. 2 (c). Especially striking is the period between 20 January 2026 and 13 February 2026, where a series of intense ARs formed and made landfall over Western Europe within a short period of time.

This series of ARs caused consistent, heavy precipitation over Portugal, Spain and Northern Africa. In January 2026, the Portuguese meteorological service IPMA reported a monthly precipitation sum of over 400 % of the expected precipitation from climatology for a region in the south of Portugal (Instituto Português do Mar e da Atmosfera, 2026b). The precipitation sum for February was even larger with more than 600 % of the normal precipitation in several regions across Portugal (Instituto Português do Mar e da Atmosfera, 2026a). The Spanish meteorological service AEMET also recorded over 300 % of the normal February precipitation across most regions of Spain in February 2026 (Agencia Estatal de Meteorología, 2026). Also the Northern African countries Morocco and Tunisia experienced unusual heavy rainfall from this series of ARs (Bett, 2026). The resulting wide spread floodings over the affected countries caused large damages: In Portugal and Spain, agricultural fields were submerged and the crop damage was estimated to be in the hundreds of millions of euros (Martinez and Nazca, 2026). Several areas had to be evacuated, such as regions in Andalusia, Spain, where 11,000 people had to leave their homes (Martinez and Nazca, 2026). Additionally, large parts of the infrastructure like streets and railway services had to be closed down (Bett, 2026).

In mid-February, the Greenland blocking weakened, allowing ETCs and their associated ARs to follow a more northerly path and make landfall over France, the United Kingdom and Ireland. These ARs had a much weaker intensity than the ones during the blocking period in late January 2026 and early February 2026.

4 Results

In this section, we analyze how well the IFS and the ICON model represented the vertical structure of the ARs sampled during the NAWDIC campaign. First, we compare the data from the IFS and the ICON models for single dropsonde observations from two NAWDIC IOPs: IOP 4 and IOP 7. Afterwards, we examine the general model performance in a statistical sense over all NAWDIC AR IOPs.

4.1 IOP 4 “Dublin”

IOP 4 “Dublin” (Fig. 3) sampled the AR, cold front and cold sector of an ETC that emerged from the US east coast on 19 January 2026. The ETC traveled eastward over the North Atlantic, until it reached France and the United Kingdom on 21 January 2026. From its initial stages, the ETC exhibited an intense AR that remained strong until it reached the eastern half

https://doi.org/10.5194/egusphere-2026-6383
Preprint. Discussion started: 9 November 2026
© Author(s) 2026. CC BY 4.0 License.

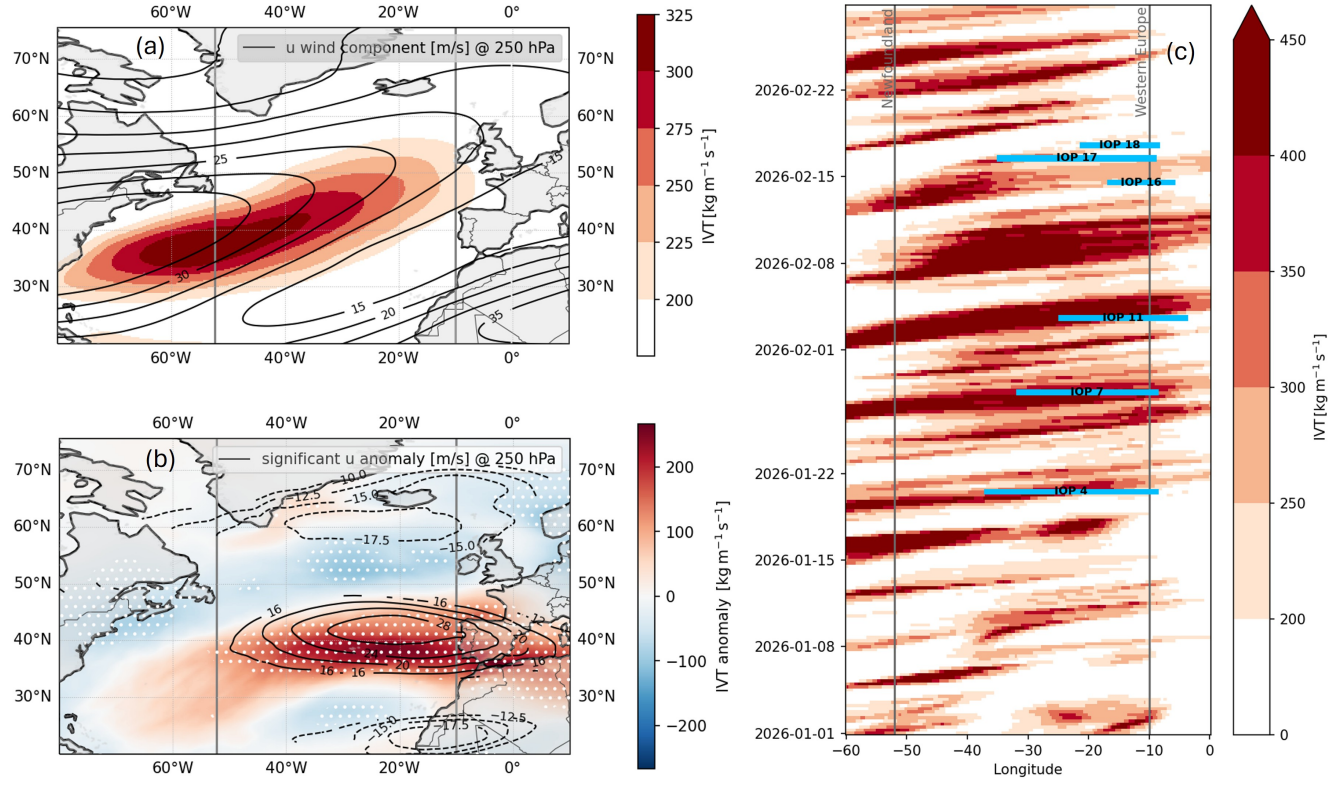


Figure 2. Panel (a): Winter month (DJF) climatology from 1984 to 2024 of ERA5 IVT in shading and the u wind component at 250 hPa in contour lines, representing ARs and the jet stream. Panel (b): Anomalies of IVT and the jet stream during the time period between 19 January to 19 February 2026, a part of the NAWDIC campaign, with respect to the 1984-2024 winter month climatology. Regions with significant IVT anomalies are marked with dots, the jet stream anomalies are only displayed in regions where they are significant. Panel (c): Hovmoeller diagram of IVT over the North Atlantic, averaged over the latitudes 30 °N - 55 °N. NAWDIC IOPs that targeted ARs are displayed in blue corresponding to their timing and their longitudinal extend.

of the North Atlantic. The AR was sampled by NAWDIC at around 30 °W, where its maximum IVT values still exceeded 1000 $\mathrm{kg\,m^{-1}\,s^{-1}}$ (Fig. 1 (a)). It weakened before reaching the European coast and made landfall on the 21 January 2026 over Portugal, the western part of France and the United Kingdom.

Figure 3 (a) displays the location of one dropsonde, marked with a circle, which was released into the core of this AR at 11:51 UTC, and was assimilated in both the IFS and ICON models. Fig. 3 (b) and (c) show the IFS and ICON feedback data, including the profile of the dropsonde observations in black, the model FG in orange and the model AN in blue.

The IFS FG (Fig. 3 (b)), aligns well with the dropsonde observation of specific humidity, horizontal wind speed and moisture flux magnitude in most vertical levels. We see a small underestimation of humidity at around 825 hPa and a larger one between 500 and 600 hPa, which are both corrected in the AN. Together with the small wind speed underestimation in the FG at the ground, and between 500 and 600 hPa, this results in an underestimation of moisture flux magnitude between 500 and 600 hPa,

https://doi.org/10.5194/egusphere-2026-6383
Preprint. Discussion started: 9 November 2026
© Author(s) 2026. CC BY 4.0 License.

where the FG only estimates half the magnitude of the observed moisture flux. In the low levels, the moisture flux magnitude is also slightly underestimated and corrected in the AN, which aligns well with the observation.

The ICON FG and AN match the dropsonde observation well (Fig. 3 (c)). The only notable deviation we observe is the slight underestimation of specific humidity in the FG between 850 and 700 hPa, which is also evident in the FG moisture flux magnitude in the same vertical level. While smaller deviations may be invisible due to the lower vertical resolution of the ICON feedback data compared to the IFS feedback data, the overall deviation between the ICON FG and the observations on the available model levels is very small for this assimilated dropsonde. Between 650 hPa and 700 hPa, a few model levels are missing in the ICON feedback data of humidity, and therefore also in the moisture flux magnitude profile. An explanation for this could be the rejection of specific model levels in the assimilation procedure.

4.2 IOP 7 "Limerick"

Another intense AR was sampled during IOP 7 "Limerick" on 28 January 2026. The AR belonged to an extratropical cyclone that developed on 27 January 2026 close to the US east coast. It was associated with a strong AR that was sampled by NAWDIC between 15 °W and 30 °W on 28 January. The AR made landfall over the Iberian Peninsula only a few hours after the flight in the night towards the 29 January 2026. The IVT values were still above 750 $\mathrm{kg\,m^{-1}\,s^{-1}}$ when the AR reached Portugal. The sampled AR followed shortly after the severe storm caused by the secondary cyclone "Kristin", which hit Portugal on the morning of 28 January (Rawnsley, 2026).

The IFS FG and AN (Fig. 4 (b)) of specific humidity resemble approximately the dropsonde observation in the lower levels up until 750 hPa. Between 750 hPa and 650 hPa, the FG specific humidity decreases much stronger with height than the observation and then stays constant at around 2-3 $\mathrm{g\,kg^{-1}}$ for the upper part of the vertical column, whereas the observation shows lower values between 500-600 hPa. The AN mostly reflects the observation. The FG horizontal wind speed matches the observation well and only shows a pronounced local underestimation of wind speed in the upper levels around 425 hPa, which is corrected in the AN. The FG of moisture flux magnitude reflects the same deviations from the observation and the AN as shown in the specific humidity. The differences between the FG and the AN moisture flux magnitude are large between 750 and 500 hPa, with the FG showing only half of the flux estimated by the observation and the AN. The same moisture underestimation in the IFS was even more pronounced a few hours later, which can be seen in the IFS feedback data for another dropsonde during IOP 7 at 15:58 UTC (compare Fig. S2 in the supplementary material), which was only assimilated in the IFS and not in the ICON model. This indicates that the IFS model consistently underestimated the vertical extent of the AR sampled in IOP 7.

The ICON FG (Fig. 4 (c)) underestimates the observed humidity for the entire column between 950 and 650 hPa. The AN is pulled closer towards the observation in these levels. Above 600 hPa, the FG humidity estimate aligns well with the observation and the AN. The wind speed of the ICON FG, AN and the observation are in close agreement with each other. The FG moisture flux magnitude shows the same underestimation as the humidity in the lower levels up to 650 hPa, but also indicates a slightly lower moisture flux in the AN than shown in the observation. Again, a few model levels are missing in the ICON feedback file. This time, the feedback data of both the humidity and the wind speed between 600 hPa and 650 hPa is affected.

https://doi.org/10.5194/egusphere-2026-6383
Preprint. Discussion started: 9 November 2026
© Author(s) 2026. CC BY 4.0 License.

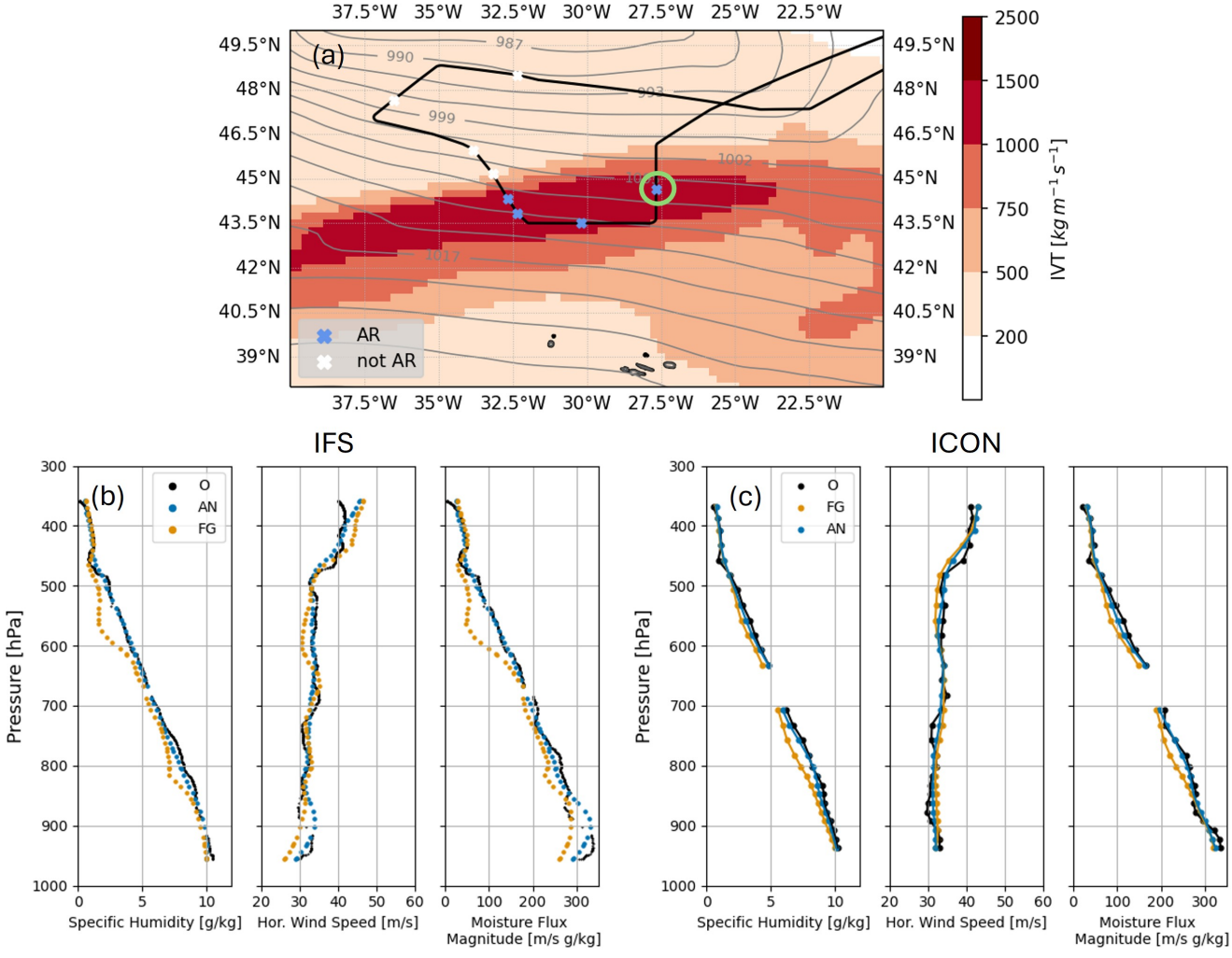


Figure 3. Case study of a selected dropsonde released into the core of the AR sampled during NAWDIC IOP 4 "Dublin" on 20 January 2026 at 11:51 UTC. Panel (a) displays the AR using ERA5 mean sea level pressure (grey lines) and IVT (red shading), valid at 12 UTC. Additionally, the HALO flight track and the dropsonde release positions are shown in (a). For the dropsonde circled in (a), the observation (O), first guess (FG) and analysis (AN) of different variables are shown for the IFS model in panel (b) and for the ICON model in panel (c).

https://doi.org/10.5194/egusphere-2026-6383
Preprint. Discussion started: 9 November 2026
© Author(s) 2026. CC BY 4.0 License.

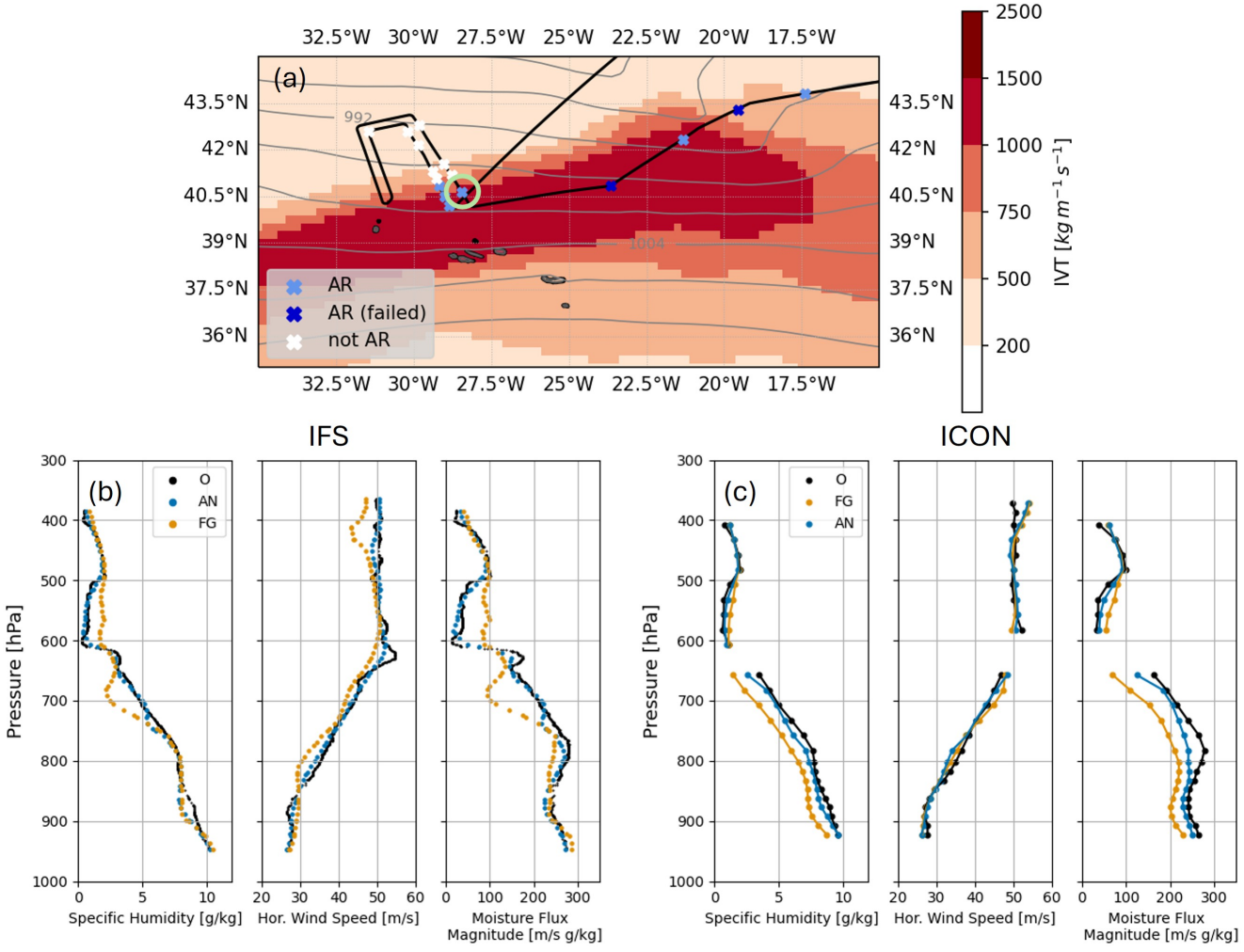


Figure 4. Same as in Fig. 3, but for a selected dropsonde released into the AR sampled during IOP 7 "Limerick" on 28 January 2026. The ERA5 IVT and mean sea level pressure are valid at 14 UTC, which matches approximately the release time of the selected drop at 13:40 UTC, circled in (a). Panel (b) shows the IFS feedback data, panel (c) the ICON feedback data.

https://doi.org/10.5194/egusphere-2026-6383
Preprint. Discussion started: 9 November 2026
© Author(s) 2026. CC BY 4.0 License.

4.3 Statistical Model Departures Over AR Regions

We now assess the performance of the IFS and ICON in representing the correct vertical AR structure in a more systematic way. To this end, we calculate the FG and AN departures across all AR dropsonde observations that were assimilated in the corresponding model.

4.3.1 IFS

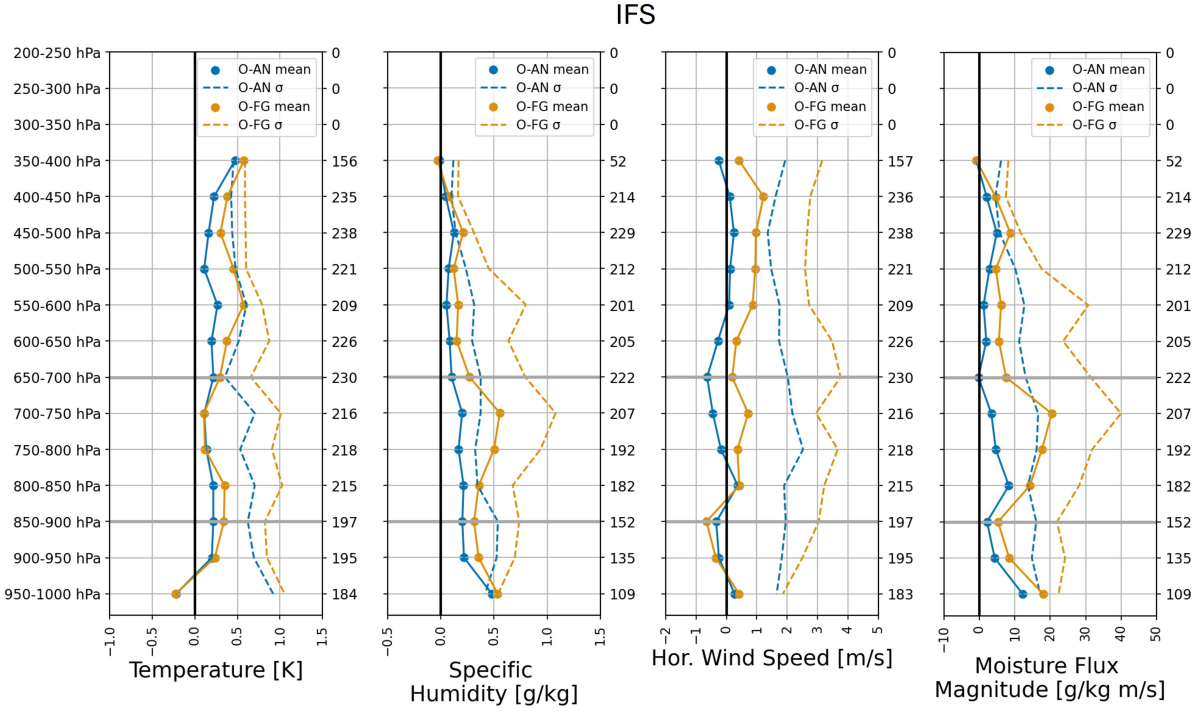


Figure 5. First guess and analysis departures (O-FG and O-AN) are displayed, computed over all NAWDIC AR dropsondes assimilated in the IFS model. For each 50 hPa wide bin, the mean and standard deviation over all departures belonging to the vertical interval is calculated for four variables: the air temperature (a), the specific humidity (b), the horizontal wind speed (c) and the moisture flux magnitude (d). The values on the right y-axis indicate the number of single departure values that went into the calculation of mean departure and standard deviation of the corresponding bin. The grey lines at 700 hPa and 900 hPa represent the boarders of the planetary boundary layer (PBL) from 1000 hPa to 900 hPa, the lower free troposphere from 900 hPa to 700 hPa and the upper free troposphere from 700 hPa to the top of the vertical column.

Fig. 5 displays the statistical departures for temperature (a), specific humidity (b), horizontal wind speed (c) and moisture flux magnitude (d) in the IFS over AR regions. The FG and AN mean departures for temperature (Fig. 5(a)) are positive between 950 hPa and 300 hPa, corresponding to a colder FG and AN than dropsonde observations across the entire vertical column above the PBL. However, the random errors are high at the lower levels and decrease only above 550 hPa.

https://doi.org/10.5194/egusphere-2026-6383
Preprint. Discussion started: 9 November 2026
© Author(s) 2026. CC BY 4.0 License.

The FG and AN mean departures for specific humidity (Fig. 5(b)) are positive throughout the entire vertical column and indicate the tendency of a too dry model compared to dropsonde observations. This is accompanied by large random errors. The discrepancies between the FG and AN departures are largest in the 700-750 hPa level. The FG underestimates the humidity on average by more than 0.5 $\mathrm{g\,kg^{-1}}$ in this level, whereas the AN departure lies only at around 0.2 $\mathrm{g\,kg^{-1}}$, comparable as in the other levels of the lower free troposphere. Also the FG random errors of specific humidity are largest in the 700-750 hPa level. In the PBL, both FG and AN show an underestimation of the specific humidity of around 0.5 $\mathrm{g\,kg^{-1}}$, which, together with small random errors, indicates a structural dry model bias in lower levels.

The mean departures in horizontal wind speed (Fig. 5 (c)) for both FG and AN hover around zero, and are rather small with values of maximum 1.2 $\mathrm{m\,s^{-1}}$, especially compared to the considerably high random errors of more than 3.5 $\mathrm{m\,s^{-1}}$. The FG and AN departures are close to each other in the lower troposphere up until 800 hPa. Above 800 hPa, the FG and AN departures show stronger deviations than in the lower levels, and the mean and random errors in the AN are strongly decreased through the data assimilation. The FG consistently estimates around 1 $\mathrm{m\,s^{-1}}$ weaker wind speeds than the AN. However, this underestimation in wind speed in the FG above 550 hPa is accompanied by large random errors.

Like the mean departures for specific humidity, the mean departures for the moisture flux magnitude (Fig. 5 (d)) are positive across almost all vertical levels, corresponding to a tendency of underestimation in moisture flux magnitude by both the FG and the AN. The largest FG departures appear in the 700-750 hPa level, which matches the level of the largest FG departures in specific humidity. The AN departures in moisture flux magnitude in this level are also positive, but much smaller than the FG departures. The random errors are highest in the 700-750 hPa level, with values of maximal 40 $\mathrm{g\,kg^{-1}\,m\,s^{-1}}$. In the PBL, the moisture flux magnitude is underestimated in the FG and AN, driven both by the underestimation in specific humidity and wind speed. Comparably small random errors in this level indicate a structural underestimation of moisture flux magnitude in the PBL.

4.3.2 ICON

The results for the ICON model are shown in Fig. 6. The ICON FG and AN mean temperature departures (Fig. 6 (a)) are positive throughout the entire vertical column, except for the PBL. In the PBL, the FG and AN departures are close to zero and lie close together. In the lower free troposphere, above 800 hPa, the FG and AN departures start to deviate from each other, with the FG stronger underestimating the temperature than the AN by around 0.25 K. The largest FG departures are reached in the upper free troposphere in the 550-600 hPa level, with almost 0.6 K. The random errors are large across all vertical levels, and only decrease in the top layers.

The specific humidity departures for FG and AN (Fig. 6 (b)) are positive in almost all vertical layers, corresponding to a slight dry bias. The AN departures are consistently smaller than the FG departures in the PBL and the lower free troposphere up to 600 hPa. Above 600 hPa, the FG and AN departures of specific humidity are small, also corresponding to generally dry air in the upper free troposphere. The largest FG departures of around 0.5 $\mathrm{g\,kg^{-1}}$ are reached in the 650-700 hPa layer and in the 850-900 hPa layer. The random errors of the specific humidity departures in the FG and AN are small compared to the random errors seen in the other variables. This provides reasonable confidence in the identified dry bias.

https://doi.org/10.5194/egusphere-2026-6383
Preprint. Discussion started: 9 November 2026
© Author(s) 2026. CC BY 4.0 License.

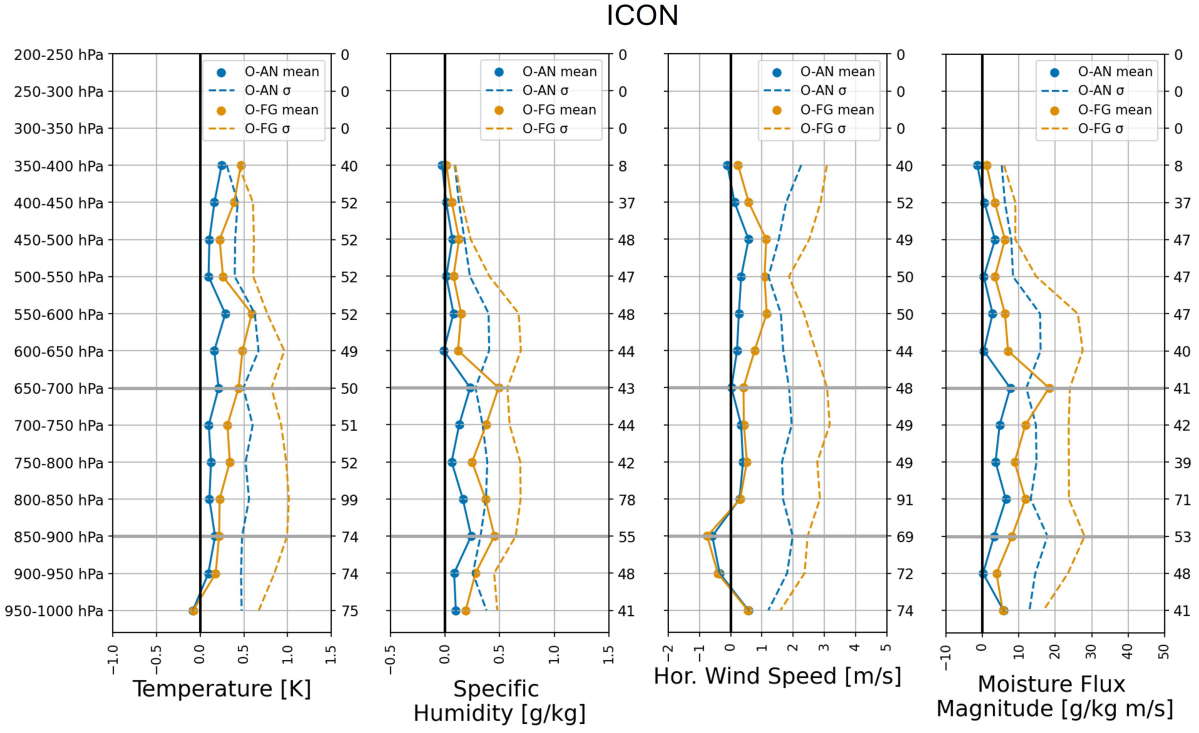


Figure 6. The same as Fig. 5, but for the ICON feedback data of AR dropsondes that were assimilated in the ICON model.

The mean wind speed departures for FG and AN (Fig. 6 (c)) are almost completely aligned throughout the PBL and the lower free troposphere, and vary between -1 and +1 $\mathrm{m\,s^{-1}}$. In the upper free troposphere above 600 hPa, the FG starts to underestimate the horizontal wind speed by over 1 $\mathrm{m\,s^{-1}}$. The AN departure in these layers is much smaller. However, the random errors in wind speed are large throughout the entire column.

The moisture flux magnitude departures (Fig. 6 (d)) are positive in both the FG and AN throughout the entire vertical column, but the AN departures are only around half as large as the FG departures. The underestimation in moisture flux magnitude results in the lower layers from the underestimation in specific humidity, and in the upper layers from the underestimation of horizontal wind speed. The largest FG underestimation of moisture flux magnitude appears in the 650-700 hPa layer and reaches almost 20 $\mathrm{g\,kg^{-1}\,m\,s^{-1}}$.

5 Discussion

Even though the IFS and ICON can generally resemble the vertical structure of ARs well, our study revealed some still existing deficiencies in the IFS and ICON model regarding the representation of North Atlantic ARs (Sect. 4.3). In both models, the random errors are consistently larger than the mean departures in almost all vertical levels and over all variables, hence we can

https://doi.org/10.5194/egusphere-2026-6383
Preprint. Discussion started: 9 November 2026
© Author(s) 2026. CC BY 4.0 License.



only carefully draw conclusions on significant, systematic biases in the two models from the NAWDIC AR dropsonde data. However, we can derive model tendencies and interpret the random errors. For both models, a slight cold and dry bias, as well as a weaker wind bias in the upper free troposphere and general high random errors in horizontal wind speed are identified. The dry and weaker wind bias leads to an underestimation of moisture flux magnitude in both models. These results are in line with findings from Yu et al. (2025), who identified in ERA5 forecasts and analysis fields a cold bias, dry bias and weaker wind bias during AR events in the winter time over mid-latitude oceans, resulting in an underestimation of moisture transport.

In the IFS, the underestimation of moisture and moisture flux magnitude found in this study is most pronounced at the upper level extension of ARs, which is usually estimated to lie at around 700 hPa (Ralph et al., 2018). Comparing the dry bias in the IFS during AR events to the dry bias considering also all other synoptic features sampled during the NAWDIC campaign (results shown in the supplementary material, Sect. S3.1), we can confirm a larger underestimation in humidity during AR events than during other conditions. We further find that the underestimation in moisture flux magnitude and the random errors in wind speed and moisture flux magnitude in the IFS are larger during AR events than during other conditions. Lavers et al. (2020a) identified a dry bias of around 0.1-0.2 $\mathrm{g\,kg^{-1}}$ below 850 hPa for eastern North Pacific ARs in the IFS model. The maximal dry bias of 0.5 $\mathrm{g\,kg^{-1}}$, we found for North Atlantic ARs, lies in the level of 700-750 hPa. This North Atlantic dry bias is located in upper tropospheric levels, and is larger than the bias found in Lavers et al. (2020a) on eastern North Pacific ARs in the IFS, even though the IFS has gone through several improvements since 2020. However, the biases can be case dependent and the bias differences might partly be due to a more strict selection criteria of AR dropsondes in this study compared to Lavers et al. (2020a), where all AR Recon dropsondes of 2018 and 2019 were included without any further selection criteria. Ramos et al. (2026) identified a dry bias of around 0.5 $\mathrm{g\,kg^{-1}}$ in 725-750 hPa for ARs over Brest in France, a location where North Atlantic ARs often make landfall, which is in line with the findings in this current study. The large random errors in moisture flux magnitude over North Atlantic ARs match the uncertainties in moisture flux magnitude described in Lavers et al. (2018) for Northeast Pacific ARs. However, the largest underestimation in moisture flux magnitude in Northeast Pacific ARs is found in the PBL (Lavers et al., 2020a), whereas over the North Atlantic, we see an underestimation in the PBL, but an even larger underestimation at the upper-level extension of ARs. This model behaviour may be specific for ARs over the North Atlantic. Lavers et al. (2020a) further identified a weaker wind bias in the IFS for Northeast Pacific ARs in the level below 950 hPa. This tendency is not clearly visible in the results of the present study on North Atlantic ARs.

Compared to the dry bias in the IFS, the underestimation of humidity in ICON is continuously visible in all layers below 600 hPa and the mean bias and random error in specific humidity is comparable between situations with and without ARs (compare to the results shown in the Appendix S3.2). Only the mean bias and random errors in moisture flux magnitude are higher in ARs than in other synoptical features. The representation of ARs in ICON has so far only been evaluated for case studies of Arctic ARs and mainly for non-operational, high-resolution ICON simulations (Bresson et al., 2022; Dorff et al., 2025). Dorff et al. (2025) found a similar vertical AR structure in high-resolution ICON simulations like in dropsonde observations of a single AR event, but the vertical variability of different variables in ICON is too small compared to observations. Dorff et al. (2025) further identified too dry estimates in the ICON model in the lowest 3 km of the troposphere, compared to observations, in this single case. Bresson et al. (2022) have shown a much better performance of ICON high-resolution simu-

https://doi.org/10.5194/egusphere-2026-6383
Preprint. Discussion started: 9 November 2026
© Author(s) 2026. CC BY 4.0 License.

lations compared to the global ICON model in representing the correct vertical structure of a selected Arctic AR. The global ICON model strongly underestimates the specific humidity in the AR core. The results of Bresson et al. (2022) and Dorff et al. (2025) agree with the dry tendency in the global ICON model over ARs. However, it is hard to compare the case studies on Arctic ARs to the performance of the operational, global ICON model for ARs over the North Atlantic ocean around 40-50 °N, which was assessed for the first time in this study.

The data assimilation procedures of both models use the observations to provide a best estimate of the atmosphere, and as such, the model draws towards the observations. As shown in the two case studies , the AN is more rigorously corrected in some cases as in others, depending on how much the FG deviates from the observations. The statistical evaluation over all AR sondes accounts for these fluctuations and we can confirm an overall successfull data analysis in both the IFS and ICON, as the mean biases and random errors are smaller in the AN than in the FG across all considered variables. However, differences between the different atmospheric levels are found: In the IFS, the FG and AN mean biases are similar to each other in the PBL and the lower free troposphere below 800 hPa, and the random errors in the AN are only slightly smaller than in the FG. Between 800 and 500 hPa, the mean biases and random errors are clearly larger in the FG than in the AN. Especially between 700 hPa and 750 hPa, the large departures in the FG of specific humidity, horizontal wind speed, and consecutively also moisture flux magnitude, are consistently corrected in the AN and the large random errors in specific humidity and moisture flux magnitude are reduced by more than half. The ICON model estimates of the specific humidity and the moisture flux magnitude improve consistently over most vertical levels through the data assimilation by a reduction of the mean and the random errors in the AN compared to the FG. The mean bias in temperature is only reduced in the lower and upper free troposphere. The AN mean bias in wind speed is only smaller than the FG bias in the upper free troposphere, where a weaker wind bias in the FG is corrected.

6 Conclusions

This study evaluated the model performance of the IFS and ICON forecasting systems regarding the representation of North Atlantic Atmospheric Rivers (ARs). It used new dropsonde observations collected by the NAWDIC campaign in January and February 2026 during research flights with the HALO research aircraft over the North Atlantic. One focal point of the NAWDIC campaign was to target ARs affecting the Western European coast, and the campaign succeeded in collecting a unique, highly vertically resolved dropsonde dataset of the vertical AR structure over the mid-latitude North Atlantic. This exceptional dataset, together with the joint effort of the ECMWF and the DWD to assimilate the dropsonde data in real time in their forecasting systems, enabled this first evaluation of North Atlantic AR representation in the IFS and ICON models. Several of the ARs sampled during the NAWDIC campaign traveled on an unusual southerly storm track towards the Iberian Peninsular and Northern Africa, and caused heavy precipitation and widespread flooding over Portugal, Spain and Morocco. Comparing the IFS and ICON models first guess (FG) and analysis (AN) to the NAWDIC dropsonde observations (O), the main conclusions regarding the two research questions are as follows:

- How well do the IFS and ICON models represent the vertical structure of selected, impactful AR events over the North Atlantic during the NAWDIC campaign?

https://doi.org/10.5194/egusphere-2026-6383
Preprint. Discussion started: 9 November 2026
© Author(s) 2026. CC BY 4.0 License.

Although the two models generally accurately represent the vertical AR structure, we find discrepancies in the model performances regarding different AR cases, ranging from close alignment to significant deviations between models and dropsonde observations. Considering all observations, we find a slight cold bias and dry bias in the IFS and ICON over AR regions. Together with large random errors in horizontal wind speed estimates and a weaker wind bias in the upper levels, this results in an underestimation of moisture flux magnitude in both models. In the IFS, the underestimation of moisture and moisture flux magnitude, accompanied by large random errors, is maximal at the upper-level extension of ARs between 700 and 750 hPa, and points to an underestimation of AR height in the IFS. In the ICON model, the underestimation of humidity and moisture flux magnitude is consistent over the entire planetary boundary layer and lower free tropopause.

- To what extent does data assimilation improve the model analysis relative to the first guess estimates over North Atlantic AR regions?

Overall, the mean biases and random errors of all variables decrease through the data assimilation, which is expected and proves a successful data assimilation procedure. In the IFS, only small improvements in the mean bias through the data assimilation are visible in the surface near planetary boundary layer and the lower free troposphere below 800 hPa. At the higher levels, the influence increases and the largest improvement through data assimilation is found between 700 and 750 hPa, where a pronounced dry bias is corrected. In the ICON model, we observe a consistent correction of the dry bias and underestimation of moisture flux magnitude over all vertical levels. The wind speed mean bias is only reduced through the data assimilation in the upper free troposphere above 600 hPa, with a correction of the weaker wind bias in the FG.

Our study provided the first evaluation of the operational IFS and ICON model performance regarding ARs over the mid-latitude North Atlantic. While the errors uncovered in the models are similar to findings of previous studies analyzing ARs in other oceanic basins or over the continents, using older and/or different versions of the IFS and ICON model, several new aspects have been identified. For instance, the IFS appears to exhibit North Atlantic specific vertical levels of highest errors that differ from findings in the Northeast Pacific.

It is important to point out that the results were derived from a comparably small amount of dropsondes from a single observational campaign, leading to a spatially and temporally limited dataset. Still, the unusual synoptical situation during the NAWDIC campaign enabled the sampling of exceptionally strong ARs with high impacts for Western Europe. However, the results are limited by the focus on a small subset of ARs that is not entirely representative for a typical North Atlantic AR season and, per definition, cannot capture inter-annual variability. Additionally, the sensors implemented in the KITsonde dropsonde system, which are the same as used in several operational radiosondes, may not be free of errors. The humidity sensors have a slightly reduced response time after falling through precipitation and mid level clouds (Kottmeier et al., 2025; Ingleby, 2017). However, this should not influence measurements at the upper-level extension of ARs, where we see the largest model errors. Considering the reduction in sensor response time with time after the release, it is estimated that the influence of this error is generally small in the mid and lower levels of the troposphere (Kottmeier et al., 2025).

Our results stress that NWP models are still facing challenges in representing such impactful atmospheric phenomena like the moisture flux in ARs, despite continuous model improvements in the last years. These deficiencies should be investigated

https://doi.org/10.5194/egusphere-2026-6383
Preprint. Discussion started: 9 November 2026
© Author(s) 2026. CC BY 4.0 License.



further, since the underestimation of moisture transported in ARs can contribute to underestimated precipitation forecasts and thus shortcomings in impact forecasts and weather warnings for the affected regions, such as the Western European coast. Future studies will examine how much an increased observational sampling over AR regions over the North Atlantic, such as performed by the NAWDIC campaign, could improve the forecasts of downstream impacts over Europe. This can be done with the help of data denial experiments, where forecasts assimilating the campaign observations are compared to forecasts, where the additional campaign observations are denied. Similar data denial studies on the impact of AR Recon dropsondes on precipitation forecasts in the US revealed huge forecast improvement (Zheng et al., 2021; DeHaan et al., 2023; Wang et al., 2026; Tallapragada et al., 2026) and lead to the operational deployment of the AR Recon campaign, which takes place nowadays every winter.

Author contributions. MK, JGP and AMR designed the study. MK and AMR performed part of the measurements. MK performed the data analysis, created the figures and wrote the first draft of the manuscript. All authors discussed the results and contributed with manuscript revisions.

Competing interests. The authors declare that they have no conflict of interest.

Acknowledgements. This work was developed under the framework of the project 'Improving Atmospheric River forecasts with enhanced observations in moisture source regions (NAWDIC-AR)' funded by the German Research Foundation (DFG, grant number: 564641009). DAL was supported by the Copernicus Climate Change Service, which is implemented by the European Centre for Medium-Range Weather Forecasts (ECMWF) on behalf of the European Union. JGP thanks the AXA Research Fund for support. AMR received support from the Helmholtz Changing Earth program. We thank the colleagues from the NAWDIC consortium for discussions, and everybody who took part in the campaign for their input and hard work. We especially thank Julian Quinting and Bastian Kirsch for all their effort to make the assimilation of the NAWDIC dropsonde measurements possible.

https://doi.org/10.5194/egusphere-2026-6383
Preprint. Discussion started: 9 November 2026
© Author(s) 2026. CC BY 4.0 License.

References

Agencia Estatal de Meteorología: Avance Climático Nacional de febrero de 2026, https://www.aemet.es/documentos/es/noticias/2026/03/avance_climatico_nacional_febrero_2026.pdf, accessed: 2026-07-17, 2026.

Barredo, J. I.: Major flood disasters in Europe: 1950–2005, Natural hazards, 42, 125–148, https://doi.org/10.1007/s11069-006-9065-2, 2007.

Bett, D.: Europe feels the impact of weeks of wet weather and freezing cold, https://www.bbc.com/weather/articles/cwy8450qkwwo, 2026.

Bjerknes, J.: On the structure of moving cyclones, Monthly Weather Review, 47, 95–99, https://doi.org/10.1175/1520-0493(1919)47<95:OTSOMC>2.0.CO;2, 1919.

Bresson, H., Rinke, A., Mech, M., Reinert, D., Schemann, V., Ebell, K., Maturilli, M., Viceto, C., Gorodetskaya, I., and Crewell, S.: Case study of a moisture intrusion over the Arctic with the ICOsahedral Non-hydrostatic (ICON) model: resolution dependence of its representation, Atmospheric Chemistry and Physics, 22, 173–196, https://doi.org/10.5194/acp-22-173-2022, 2022.

Browning, K.: Radar measurements of air motion near fronts, Weather, 26, 320–340, https://doi.org/10.1002/j.1477-8696.1971.tb04211.x, 1971.

Carlson, T. N.: Airflow through midlatitude cyclones and the comma cloud pattern, Monthly Weather Review, 108, 1498–1509, https://doi.org/10.1175/1520-0493(1980)108<1498:ATMCAT>2.0.CO;2, 1980.

Dacre, H. F. and Clark, P. A.: A kinematic analysis of extratropical cyclones, warm conveyor belts and atmospheric rivers, npj Climate and Atmospheric Science, 8, 97, https://doi.org/10.1038/s41612-025-00942-z, 2025.

Dacre, H. F., Clark, P. A., Martinez-Alvarado, O., Stringer, M. A., and Lavers, D. A.: How do atmospheric rivers form?, Bulletin of the American Meteorological Society, 96, 1243–1255, https://doi.org/10.1175/BAMS-D-14-00031.1, 2015.

DeFlorio, M. J., Waliser, D. E., Guan, B., Lavers, D. A., Ralph, F. M., and Vitart, F.: Global assessment of atmospheric river prediction skill, Journal of Hydrometeorology, 19, 409–426, https://doi.org/10.1175/JHM-D-17-0135.1, 2018.

DeHaan, L. L., Wilson, A. M., Kawzenuk, B., Zheng, M., Monache, L. D., Wu, X., Lavers, D. A., Ingleby, B., Tallapragada, V., Pappenberger, F., et al.: Impacts of dropsonde observations on forecasts of atmospheric rivers and associated precipitation in the NCEP GFS and ECMWF IFS models, Weather and Forecasting, 38, 2397–2413, https://doi.org/10.1175/WAF-D-23-0025.1, 2023.

Desroziers, G., Berre, L., Chapnik, B., and Poli, P.: Diagnosis of observation, background and analysis-error statistics in observation space, Quarterly Journal of the Royal Meteorological Society, 131, 3385–3396, https://doi.org/10.1256/qj.05.108, 2005.

Dorff, H., Ewald, F., Konow, H., Mech, M., Ori, D., Schemann, V., Walbröl, A., Wendisch, M., and Ament, F.: Moisture budget estimates derived from airborne observations in an Arctic atmospheric river during its dissipation, Atmospheric Chemistry and Physics, 25, 8329–8354, https://doi.org/10.5194/acp-25-8329-2025, 2025.

DWD: ICON release 2025.10, https://doi.org/10.35089/WDCC/IconRelease2025.10, 2025.

ECMWF: IFS Documentation CY49R1 - Part II: Data assimilation, https://doi.org/10.21957/105cb1333c, 2024.

ECMWF: Implementation of IFS Cycle 49r1, https://confluence.ecmwf.int/spaces/FCST/pages/414584216/Implementation+of+IFS+Cycle+49r1, accessed: 2026-09-23, 2025.

ECMWF: 2025 forecast evaluation met with positive feedback, https://www.ecmwf.int/en/about/media-centre/news/2026/2025-forecast-evaluation, accessed: 2026-09-23, 2026.

Eiras-Barca, J., Lorenzo, N., Taboada, J., Robles, A., and Miguez-Macho, G.: On the relationship between atmospheric rivers, weather types and floods in Galicia (NW Spain), Natural Hazards and Earth System Sciences, 18, 1633–1645, https://doi.org/10.5194/nhess-18-1633-2018, 2018.

https://doi.org/10.5194/egusphere-2026-6383
Preprint. Discussion started: 9 November 2026
© Author(s) 2026. CC BY 4.0 License.

Ferreira, T. M., Trigo, R. M., Gaspar, T. H., Pinto, J. G., and Ramos, A. M.: The record-breaking precipitation event of December 2022 in Portugal, Natural Hazards and Earth System Sciences, 25, 609–623, https://doi.org/10.5194/nhess-25-609-2025, 2025.

Ferreira, T. M., Gaspar, T. H., Molina, M. O., Trigo, R. M., Deus, R., and Ramos, A. M.: Extreme rainfall in Madeira: the June 2023 weather event, Weather, 81, 164–171, https://doi.org/10.1002/wea.7786, 2026.

Fink, A. H., Brücher, T., Ermert, V., Krüger, A., and Pinto, J. G.: The European storm Kyrill in January 2007: synoptic evolution, meteorological impacts and some considerations with respect to climate change, Natural Hazards and Earth System Sciences, 9, 405–423, https://doi.org/10.5194/nhess-9-405-2009, 2009.

Grams, C. M.: A life cycle definition of year-round weather regimes in the North Atlantic European region, EGUsphere, 2026, 1–60, https://doi.org/10.5194/wcd-7-1641-2026, 2026.

Graw: Radiosonde DFM-17, High accuracy GNSS radiosonde with PTU measurements, https://www.graw.de/fileadmin/cms_upload/en/Resources/pdf/DB-DFM-17-DE_V02.00.pdf, accessed: 2026-08-19, 2025.

Harvey, B., Methven, J., Sanchez, C., and Schäfler, A.: Diabatic generation of negative potential vorticity and its impact on the North Atlantic jet stream, Quarterly Journal of the Royal Meteorological Society, 146, 1477–1497, https://doi.org/10.1002/qj.3747, 2020.

Hersbach, H., Bell, B., Berrisford, P., Hirahara, S., Horányi, A., Muñoz-Sabater, J., Nicolas, J., Peubey, C., Radu, R., Schepers, D., et al.: The ERA5 global reanalysis, Quarterly journal of the royal meteorological society, 146, 1999–2049, https://doi.org/10.1002/qj.3803, 2020.

Hofstätter, M., Lexer, A., Homann, M., and Blöschl, G.: Large-scale heavy precipitation over central Europe and the role of atmospheric cyclone track types, International Journal of Climatology, 38, e497–e517, https://doi.org/10.1002/joc.5386, 2018.

Ingleby, B.: An assessment of different radiosonde types 2015/2016, Technical Memorandum 807, European Centre for Medium-Range Weather Forecasts (ECMWF), Reading, United Kingdom, https://doi.org/10.21957/0nje0wpsa, accessed: 2026-07-31, 2017.

Instituto Português do Mar e da Atmosfera: Boletim Climatológico – Fevereiro 2026, https://www.ipma.pt/resources.www/docs/im.publicacoes/edicoes.online/20260316/upSTvEDqNFQRtdDSssWr/cli_20260201_20260228_pcl_mm_co_pt.pdf, accessed: 2026-07-17, 2026a.

Instituto Português do Mar e da Atmosfera: Boletim Climatológico – Janeiro 2026, https://www.ipma.pt/resources.www/docs/im.publicacoes/edicoes.online/20260313/FvTHXCNlkkXzTHuuxaHk/cli_20260101_20260131_pcl_mm_co_pt.pdf, accessed: 2026-07-17, 2026b.

Ionita, M., Nagavciuc, V., and Guan, B.: Rivers in the sky, flooding on the ground: the role of atmospheric rivers in inland flooding in central Europe, Hydrology and Earth System Sciences, 24, 5125–5147, https://doi.org/10.5194/hess-24-5125-2020, 2020.

Kalnay, E.: Atmospheric modeling, data assimilation and predictability, Cambridge University Press, https://doi.org/10.1017/9780511920608, 2003.

Kottmeier, C., Wieser, A., Corsmeier, U., Kalthoff, N., Gasch, P., Kirsch, B., Ebert, D., Ulanowski, Z., Schell, D., Franke, H., et al.: A new versatile dropsonde for atmospheric soundings–the KITsonde, Atmospheric Measurement Techniques, 18, 3161–3178, https://doi.org/10.5194/amt-18-3161-2025, 2025.

Lavers, D. A., Rodwell, M. J., Richardson, D. S., Ralph, F. M., Doyle, J. D., Reynolds, C. A., Tallapragada, V., and Pappenberger, F.: The gauging and modeling of rivers in the sky, Geophysical Research Letters, 45, 7828–7834, https://doi.org/10.1029/2018GL079019, 2018.

Lavers, D. A., Ingleby, N. B., Subramanian, A. C., Richardson, D. S., Ralph, F. M., Doyle, J. D., Reynolds, C. A., Torn, R. D., Rodwell, M. J., Tallapragada, V., et al.: Forecast errors and uncertainties in atmospheric rivers, Weather and Forecasting, 35, 1447–1458, https://doi.org/10.1175/WAF-D-20-0049.1, 2020a.

https://doi.org/10.5194/egusphere-2026-6383
Preprint. Discussion started: 9 November 2026
© Author(s) 2026. CC BY 4.0 License.

Lavers, D. A., Ralph, F. M., Richardson, D. S., and Pappenberger, F.: Improved forecasts of atmospheric rivers through systematic reconnaissance, better modelling, and insights on conversion of rain to flooding, Communications Earth & Environment, 1, 39, https://doi.org/10.1038/s43247-020-00042-1, 2020b.

Ludwig, P., Ehmele, F., Franca, M. J., Mohr, S., Caldas-Alvarez, A., Daniell, J. E., Ehret, U., Feldmann, H., Hundhausen, M., Knippertz, P., Küpfer, K., Kunz, M., Mühr, B., Pinto, J. G., Quinting, J., Schäfer, A. M., Seidel, F., and Wisotzky, C.: A multi-disciplinary analysis of the exceptional flood event of July 2021 in central Europe – Part 2: Historical context and relation to climate change, Natural Hazards and Earth System Sciences, 23, 1287–1311, https://doi.org/10.5194/nhess-23-1287-2023, 2023.

Marchi, L., Borga, M., Preciso, E., and Gaume, E.: Characterisation of selected extreme flash floods in Europe and implications for flood risk management, Journal of Hydrology, 394, 118–133, https://doi.org/10.1016/j.jhydrol.2010.07.017, 2010.

Martinez, G. and Nazca, J.: Farmers report catastrophic damage to crops as Storm Marta hits Spain and Portugal, https://www.bbc.com/weather/articles/cwy8450qkwwo, 2026.

Martínez-Alvarado, O., Baker, L. H., Gray, S. L., Methven, J., and Plant, R. S.: Distinguishing the cold conveyor belt and sting jet airstreams in an intense extratropical cyclone, Monthly Weather Review, 142, 2571–2595, https://doi.org/10.1175/MWR-D-13-00348.1, 2014.

Mech, M., Ehrlich, A., Herber, A., Lüpkes, C., Wendisch, M., Becker, S., Boose, Y., Chechin, D., Crewell, S., Dupuy, R., et al.: MOSAiC-ACA and AFLUX-Arctic airborne campaigns characterizing the exit area of MOSAiC, Scientific data, 9, 790, https://doi.org/10.1038/s41597-022-01900-7, 2022.

Merz, B., Kuhlicke, C., Kunz, M., Pittore, M., Babeyko, A., Bresch, D. N., Domeisen, D. I., Feser, F., Koszalka, I., Kreibich, H., et al.: Impact forecasting to support emergency management of natural hazards, Reviews of geophysics, 58, e2020RG000 704, https://doi.org/10.1029/2020RG000704, 2020.

Paprotny, D., Sebastian, A., Morales-Nápoles, O., and Jonkman, S. N.: Trends in flood losses in Europe over the past 150 years, Nature communications, 9, https://doi.org/10.1038/s41467-018-04253-1, 2018.

Quinting, J., Grams, C. M., Kirsch, B., Oertel, A., Ramos, A. M., Raveh-Rubin, S., and Schäfler, A.: Dry intrusion connects high-impact cyclones Eunice and Franklin: emerging observational targets of NAWDIC, Bulletin of the American Meteorological Society, 107, E1302–E1314, https://doi.org/10.1175/BAMS-D-25-0170.1, 2026.

Rabier, F.: Overview of global data assimilation developments in numerical weather-prediction centres, Quarterly Journal of the Royal Meteorological Society, 131, 3215–3233, https://doi.org/10.1256/qj.05.129, 2005.

Rabier, F., Järvinen, H., Klinker, E., Mahfouf, J.-F., and Simmons, A.: The ECMWF operational implementation of four-dimensional variational assimilation. I: Experimental results with simplified physics, Quarterly Journal of the Royal Meteorological Society, 126, 1143–1170, https://doi.org/10.1002/qj.49712656415, 2000.

Ralph, F. M., Dettinger, M. D., Cairns, M. M., Galarneau, T. J., and Eylander, J.: Defining “atmospheric river”: How the Glossary of Meteorology helped resolve a debate, Bulletin of the American Meteorological Society, 99, 837–839, https://doi.org/10.1175/BAMS-D-17-0157.1, 2018.

Ralph, F. M., Cannon, F., Tallapragada, V., Davis, C. A., Doyle, J. D., Pappenberger, F., Subramanian, A., Wilson, A. M., Lavers, D. A., Reynolds, C. A., et al.: West Coast forecast challenges and development of atmospheric river reconnaissance, Bulletin of the American Meteorological Society, 101, E1357–E1377, https://doi.org/10.1175/BAMS-D-19-0183.1, 2020.

Ramos, A. M., Nieto, R., Tomé, R., Gimeno, L., Trigo, R. M., Liberato, M. L., and Lavers, D. A.: Atmospheric rivers moisture sources from a Lagrangian perspective, Earth System Dynamics, 7, 371–384, https://doi.org/10.5194/esd-7-371-2016, 2016.

https://doi.org/10.5194/egusphere-2026-6383
Preprint. Discussion started: 9 November 2026
© Author(s) 2026. CC BY 4.0 License.



Ramos, A. M., Sousa, P. M., Dutra, E., and Trigo, R. M.: Predictive skill for atmospheric rivers in the western Iberian Peninsula, Natural Hazards and Earth System Sciences, 20, 877–888, https://doi.org/10.5194/nhess-20-877-2020, 2020.

Ramos, A. M., Lemburg, A., Lavers, D. A., Tomé, R., and Pinto, J. G.: Assessment of the ECMWF Data Assimilation System Using Radiosonde Profiles During Atmospheric River Events Over Western Europe, Atmospheric Science Letters, 27, https://doi.org/https://doi.org/10.1002/asl2.70034, 2026.

Rawnsley, J.: At least five killed after Storm Kristin hits Portugal, www.bbc.com/news/articles/c205yl3kvzmo, accessed: 2026-09-22, 2026.

Reinert, D., Prill, F., Frank, H., Denhard, M., Baldauf, M., Schraff, C., Gebhardt, C., Marsigli, C., Förstner, J., Zängl, G., Schlemmer, L., Blahak, U., and Welzbacher, C.: DWD Database Reference for the Global and Regional ICON and ICON-EPS Forecasting System, Version 2.2.5, DWD 2026, 2026.

Santos, J. A., Woollings, T., and Pinto, J. G.: Are the winters 2010 and 2012 archetypes exhibiting extreme opposite behavior of the North Atlantic jet stream?, Monthly Weather Review, 141, 3626–3640, https://doi.org/10.1175/MWR-D-13-00024.1, 2013.

Schäfler, A., Craig, G., Wernli, H., Arbogast, P., Doyle, J. D., McTaggart-Cowan, R., Methven, J., Rivière, G., Ament, F., Boettcher, M., et al.: The North Atlantic waveguide and downstream impact experiment, Bulletin of the American Meteorological Society, 99, 1607–1637, https://doi.org/10.1175/BAMS-D-17-0003.1, 2018.

Schäfler, A., Harvey, B., Methven, J., Doyle, J. D., Rahm, S., Reitebuch, O., Weiler, F., and Witschas, B.: Observation of jet stream winds during NAWDEX and characterization of systematic meteorological analysis errors, Monthly Weather Review, 148, 2889–2907, https://doi.org/10.1175/MWR-D-19-0229.1, 2020.

Schultz, D. M.: Reexamining the cold conveyor belt, Monthly Weather Review, 129, 2205–2225, https://doi.org/10.1175/1520-0493(2001)129<2205:RTCCB>2.0.CO;2, 2001.

Schultz, D. M., Bosart, L. F., Colle, B. A., Davies, H. C., Dearden, C., Keyser, D., Martius, O., Roebber, P. J., Steenburgh, W. J., Volkert, H., et al.: Extratropical cyclones: A century of research on meteorology's centerpiece, Meteorological monographs, 59, 16–1, https://doi.org/10.1175/AMSMONOGRAPHS-D-18-0015.1, 2019.

Tallapragada, V., Wu, X., Zheng, M., Delle Monache, L., Ralph, F. M., Wu, K., Wang, X., Nageswararao, M., Wang, J., Wilson, A. M., et al.: Evaluation of GFSv16 for near-real-time data impact studies during the atmospheric river reconnaissance program 2022, Journal of Geophysical Research: Atmospheres, 131, https://doi.org/10.1029/2025JD044818, 2026.

Waliser, D. and Guan, B.: Extreme winds and precipitation during landfall of atmospheric rivers, Nature Geoscience, 10, 179–183, https://doi.org/10.1038/ngeo2894, 2017.

Wang, J., Lavers, D. A., Delle Monache, L., Ingleby, B., Zheng, M., Wu, X., Ralph, F. M., and Pappenberger, F.: Impacts of atmospheric river reconnaissance dropsondes on ECMWF Integrated Forecasting System precipitation forecasts, Quarterly Journal of the Royal Meteorological Society, 152, https://doi.org/10.1002/qj.70019, 2026.

Wendisch, M., Macke, A., Ehrlich, A., Lüpkes, C., Mech, M., Chechin, D., Dethloff, K., Velasco, C. B., Bozem, H., Brückner, M., et al.: The Arctic cloud puzzle: Using ACLOUD/PASCAL multiplatform observations to unravel the role of clouds and aerosol particles in Arctic amplification, Bulletin of the American Meteorological Society, 100, 841–871, https://doi.org/10.1175/BAMS-D-18-0072.1, 2019.

Wendisch, M., Crewell, S., Ehrlich, A., Herber, A., Kirbus, B., Lüpkes, C., Mech, M., Abel, S. J., Akansu, E. F., Ament, F., et al.: Overview: quasi-Lagrangian observations of Arctic air mass transformations–introduction and initial results of the HALO–(AC) 3 aircraft campaign, Atmospheric Chemistry and Physics, 24, 8865–8892, https://doi.org/10.5194/acp-24-8865-2024, 2024.

Wick, G. A., Dunion, J. P., Walker, J., and Black, P. G.: Sensing Hazards with Operational Unmanned Technology: 2015–2016 Campaign Summary, Final Report, https://doi.org/10.7289/V5/TM-OAR-UAS-001, 2018.

https://doi.org/10.5194/egusphere-2026-6383
Preprint. Discussion started: 9 November 2026
© Author(s) 2026. CC BY 4.0 License.



Young, M., Monk, G., and Browning, K.: Interpretation of satellite imagery of a rapidly deepening cyclone, Quarterly Journal of the Royal Meteorological Society, 113, 1089–1115, https://doi.org/10.1002/qj.49711347803, 1987.

Yu, Q., Spensberger, C., Magnusson, L., and Spengler, T.: Forecast errors attributed to synoptic features, Meteorological Applications, 32, https://doi.org/10.1002/met.70093, 2025.

Zängl, G., Reinert, D., Rípodas, P., and Baldauf, M.: The ICON (ICOsahedral Non-hydrostatic) modelling framework of DWD and MPI-M: Description of the non-hydrostatic dynamical core, Quarterly Journal of the Royal Meteorological Society, 141, 563–579, https://doi.org/10.1002/qj.2378, 2015.

Zhang, Z., Ralph, F. M., and Zheng, M.: The relationship between extratropical cyclone strength and atmospheric river intensity and position, Geophysical Research Letters, 46, 1814–1823, https://doi.org/10.1029/2018GL079071, 2019.

Zheng, M., Delle Monache, L., Cornuelle, B. D., Ralph, F. M., Tallapragada, V. S., Subramanian, A., Haase, J. S., Zhang, Z., Wu, X., Murphy, M. J., et al.: Improved forecast skill through the assimilation of dropsonde observations from the atmospheric river reconnaissance program, Journal of Geophysical Research: Atmospheres, 126, https://doi.org/10.1029/2021JD034967, 2021.

Zheng, M., Ralph, F. M., Tallapragada, V., Wilson, A. M., Babbitt, S. H., Bartlett, S. M., Cao, B., Centurioni, L., Cordeira, J. M., Davis, C., et al.: Atmospheric River Reconnaissance: Mission Planning, Execution, and Incorporation of Operational and Science Objectives, Bulletin of the American Meteorological Society, 106, E2243–E2275, https://doi.org/10.1175/BAMS-D-24-0160.1, 2025.